

Assessing postural instability during cerebral hypoperfusion using sub-millimeter monocular 3D sway tracking

Robert Amelard^{*1}, Kevin R Murray^{1,2}, Eric T Hedge^{1,2}, Taylor W Cleworth^{1,2}, Mamiko Noguchi², Andrew Laing^{1,2}, and Richard L Hughson^{1,2}

¹Schlegel-UW Research Institute for Aging, Waterloo ON N2J 0E2, Canada

²Department of Kinesiology, University of Waterloo, Waterloo ON N2L 3G1, Canada.

Abstract

Postural instability is prevalent in aging and neurodegenerative disease, decreasing quality of life and independence. Quantitatively monitoring balance control is important for assessing treatment efficacy and rehabilitation progress. However, existing technologies for assessing postural sway are complex and expensive, limiting their widespread utility. Here, we propose a monocular imaging system capable of assessing sub-millimeter 3D sway dynamics. By physically embedding anatomical targets with known *a priori* geometric models, 3D central and upper body kinematic motion was automatically assessed through geometric feature tracking and 3D kinematic motion inverse estimation from a set of 2D frames. Sway was tracked in 3D and compared between control and hypoperfusion conditions. The proposed system demonstrated high agreement with a commercial motion capture system (error $4.4 \times 10^{-16} \pm 0.30$ mm, $r^2 = 0.9773$). Significant differences in sway dynamics were observed in early stance central anterior-posterior sway (control: 147.1 ± 7.43 mm, hypoperfusion: 177.8 ± 15.3 mm; $p = 0.039$) and mid stance upper body coronal sway (control: 106.3 ± 5.80 mm, hypoperfusion: 128.1 ± 18.4 mm; $p = 0.040$) commensurate with cerebral blood flow (CBF) perfusion deficit, followed by recovered sway dynamics during late stance governed by CBF recovery. This inexpensive single-camera system enables quantitative 3D sway monitoring for assessing neuromuscular balance control in weakly constrained environments.

1 Introduction

Postural control is crucial for maintaining independence and quality of life. The two components of posture, orientation and balance, require continual adjustment and coordination between afferent sensory inputs and neuromuscular control [1, 2, 3]. Aging and neurodegenerative diseases (e.g., Parkinson’s disease, multiple sclerosis) can cause deterioration in postural control, which is associated with increased risk of falls, and thus decreased quality of life [4, 5, 6]. Dual-task, attention, and cortical recording paradigms have demonstrated the involvement of higher cortical centers during balance control [7]. Therefore, potential underlying mechanisms to age-related balance decline may include decreased cortical function from low cerebral perfusion.

An underlying mechanism for unsteadiness and falls in older adults is low cerebral blood flow (CBF) from impaired cardio- or cerebrovascular regulation [8, 9, 10]. Two factors commonly affected by underlying disease pathophysiology are cerebral perfusion pressure (CPP) and arterial partial pressure of carbon dioxide ($P_a\text{CO}_2$) [11]. Cerebral autoregulation maintains relatively constant CBF across a range of CPP, but rapid changes in arterial blood pressure, such as during a supine to stand transition, can result in an acute reduction of CPP, and subsequent reduction in blood flow to the brain. This reduction in perfusion causes a decrease in energy metabolism and activity in the brain and central nervous system [12], which may affect cardio-postural balance control [13]. There is a clinical need to objectively monitor posture and balance control for assessing treatment efficacy and rehabilitation [14].

Balance control has been largely investigated by accurately measuring variation in center of pressure (CoP) and center of mass (CoM). Laboratory grade measurement technologies have traditionally been restricted to assessment in controlled environments and to validate novel technologies, but are often too

expensive or cumbersome to incorporate within clinical settings. Camera-based systems have traditionally been used to assess CoM sway. Specifically, marker-based motion capture systems have been widely used for estimating and tracking CoM during standing and locomotion, in which participants are fitted with retroreflective or actively illuminated markers and 3D kinematic data of body segments are tracked by a multi-camera laboratory setup. Although these systems are able to assess whole body motion, system expense, setup burden, and technical expertise have limited their clinical utility [15, 16]. Less expensive multimodal alternatives using an iPad and 3D camera with retroreflective markers have been proposed for static posture assessment during lying posture [17], but currently lack the ability to track dynamic sway in standing. Markerless technologies, such as multi-camera voxel reconstruction [18] and Microsoft Kinect-based technologies [19, 20], have the benefit of ambient imaging without markers, but have demonstrated insufficient accuracy for clinical utility. Nevertheless, computer vision solutions for human pose estimation have shown tremendous promise in other motion-based applications, such as activity and gesture recognition. Although applications have largely been restricted to estimation in 2D space, integrating *a priori* kinematic models with camera parameters has shown strong performance in 3D anatomical tracking of the hand joints [21] and arm [22]. The ability to accurately capture and track postural change dynamics associated with falls-related factors (such as CBF in aging) using low cost technical advances would be clinically useful for identifying an individual’s potential falls risk beyond subjective assessment.

In this paper, we propose a monocular 3D motion tracking imaging system for assessing sub-millimeter 3D sway dynamics. This system was designed to enable postural assessment in clinical or naturalistic environments as it does not require a complex setup. Using a one-time camera calibration procedure, 3D temporal upper body and central sway coordinates were assessed using a single-view (monocular) camera by fitting a kinematic model to automatically track salient target features with known *a priori* geometric target models. These *a priori* models enable higher spatial accuracy estimation compared to unsupervised 3D estimation methods by fitting a kinematic target motion model to the data. Data were transformed from the camera coordinate system into an anatomical Euclidean space to isolate sway in relevant biomechanical axes (anterior-posterior, medial-lateral, superior-inferior) by inferring absolute scene orientation. Using the lumbar kinematic matrix, a virtual central sway coordinate was projected into the body to track central sway alongside upper body sway at the shoulder. This two-factor model (central and upper body) was used to assess sway characteristics in normal and compromised cerebral perfusion (hypoperfusion) cases by tracking sway characteristics in anatomical planes.

2 Methods

2.1 Data Collection

Fourteen young healthy adults (9/5 male/female, age 24.7 ± 4.3 , mass 74.3 ± 11.7 kg) free from a history of cardiovascular, neurological and musculoskeletal disorders completed testing. Participants were instructed to refrain from caffeine and food consumption 2 hr prior to testing, and alcohol and strenuous exercise 24 hr before the laboratory visit. Study protocols and procedures were approved by a University of Waterloo Research Ethics Committee and conformed to the Declaration of Helsinki (ORE 19831). All participants provided written informed consent before testing procedures.

Participants were pseudorandomized to complete two repeated trials: (1) supine to stand transition followed by 60 s of quiet standing, and (2) 2 min of voluntary guided hyperventilation (20 breaths/min), immediately followed by a supine to stand transition and 60 s of quiet standing. In accordance with the French Posturology Association guidelines, participants were instructed to stand without shoes, with their heels 2 cm apart, and feet angled at 30° [23]. Participants were instructed to keep their eyes closed and arms crossed to eliminate afferent visual feedback and reduce anticipatory arm movement [24]. During hyperventilation, participants were coached on depth of breathing to attain a drop of at least 10 mmHg end-tidal PCO_2 (P_{ETCO_2}), which was used as a proxy for P_aCO_2 .

At the start of each testing session, anthropomorphic data were collected. Participants were then instrumented with an electrocardiogram to measure heart rate (Pilot 9200; Colin Medical Instruments, San Antonio, TX, USA), continuous arterial blood pressure finger plethysmograph to estimate cardiac stroke volume via Modelflow (Finapres Pro; FMS, Amsterdam, The Netherlands), transcranial Doppler ultrasound (WAKIe; Atys Medical, Soucieu en Jarrest, France), which insonated the right middle cerebral artery to

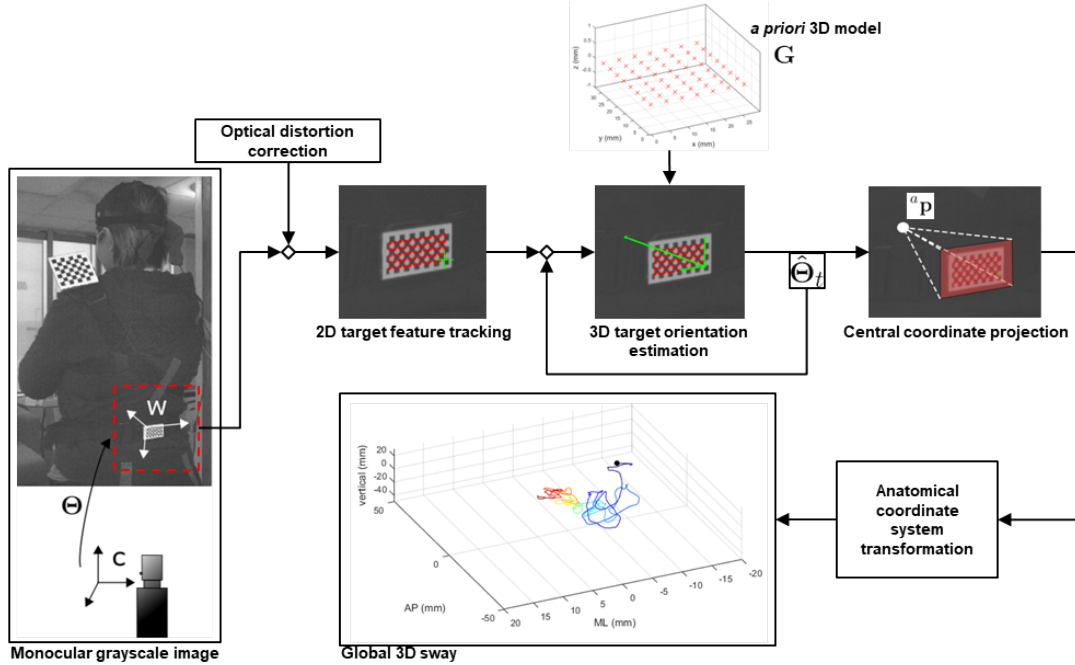


Figure 1: Overview of the monocular 3D sway estimation imaging system. Frames were captured posterior to the participant. Target features were tracked in 2D, and using *a priori* 3D geometric model, 3D sway coordinates were estimated and transformed into anatomical space. Upper body and lumbar sway coordinates were tracked, resulting in a global 3D sway profile (blue: early stance, red: late stance).

estimate CBF, and a nasal cannula connected to a capnograph to measure $P_{ET}CO_2$ (CD-3A CO_2 Analyzer, AMETEK Inc., Pittsburgh, PA, USA). Additionally, a spatially resolved near infrared spectroscopy probe (Portalite; Artinis Medical Systems, Elst, The Netherlands) was placed on the forehead above the right eye brow to measure cerebral tissue oxygenation index (TSI). Arterial blood pressure, stroke volume (SV), ECG, $P_{ET}CO_2$, and cerebral blood flow velocity (CBFv) were recorded at 1000 Hz (PowerLab, LabChart, version 7.3.7; ADInstruments, Colorado Springs, CO). After instrumentation, participants assumed a supine position for 10 min before finger blood pressure was calibrated.

2.2 Single-View 3D Sway Tracking

The main goal was to develop a monocular imaging system for tracking 3D sway characteristics to assess balance control in weakly constrained (non-laboratory) environments. The problem was posed as a single-view *a priori* geometric model and inverse kinematic estimation problem with embedded anatomical target models. Figure 1 depicts an overview of the imaging system. A temporal sequence of 3D sway coordinates $\mathbf{z}_i \in \mathbb{R}^3$ was sought from a single sequence of 2D frames, where sway is represented across the anterior-posterior (AP), medial-lateral (ML), and superior-inferior (SI) axes. Given a video from a single posterior-facing camera, model feature coordinates from a shoulder and lumbar target were automatically tracked in 2D calibrated camera space (Section 2.2.1). Then, using known *a priori* target model geometries, we fit a kinematic model to estimate the absolute sway position in 3D camera space (Section 2.2.2). Finally, we projected the lumbar kinematic orientation into the center of the body to track a virtual central sway coordinate. These coordinates were transformed into anatomical Euclidean space described by the AP, ML, SI axes (Section 2.2.3).

2.2.1 Model Feature Tracking

We adopted a two-factor hinged biomechanical model of motion, with hinging effects between central and upper body sway. To separate sway from these two components, unique anatomical targets were affixed to

the left shoulder and lumbar. Since differences in balance control result in central sway differences on the order of millimeters [25], 3D tracking estimation was guided by *a priori* geometric models to increase 3D estimation accuracy. The mathematical formulation presented here is generalizable to asymmetric target models with known root-relative feature coordinates. This asymmetry guarantees an orientation-dependent unique mapping onto 2D image space.

A single monocular grayscale camera (GS3-U3-41C6NIR, FLIR) was positioned 1 m behind the participant. Due to the high accuracy requirements of the system, optical distortions were estimated once and removed frame-by-frame using a two-step global-local camera calibration procedure [26]. Images of a planar checkerboard pattern were recorded, and intrinsic and extrinsic camera parameters were modeled as a linear projection from 3D world coordinates to 2D image coordinates:

$$\alpha {}^o\mathbf{X} = \mathbf{K} {}^c_w\mathbf{M} {}^w\mathbf{X} \quad (1)$$

where α is an arbitrary scale parameter, ${}^o\mathbf{X}$ and ${}^w\mathbf{X}$ are the checkerboard corner coordinates in the image plane and world coordinate system respectively, ${}^c_w\mathbf{M}$ is the extrinsic transformation matrix from 3D world to 3D camera coordinates, and \mathbf{K} is the intrinsic camera matrix:

$$\mathbf{K} = \begin{bmatrix} f_x & s & x_0 \\ 0 & f_y & y_0 \\ 0 & 0 & 1 \end{bmatrix} \quad (2)$$

where (f_x, f_y) is the focal length, s is skew, and (x_0, y_0) is the principle point in the image plane. This matrix is fixed for the camera, and will be used later for estimating sway target positions. From this, we can define the world-to-image projection transformation function:

$$\Pi({}^w\mathbf{X}) = \frac{1}{\alpha} \mathbf{K} {}^c_w\mathbf{M} {}^w\mathbf{X} \quad (3)$$

The optical field distortion was estimated by refining the closed-form solution using nonlinear least squares minimization of a two-coefficient radial distortion [26, 27]. This parameterization was used to undistort each frame prior to spatial processing to guarantee distance-independent homogeneous pixel spacing, and thus accurate sway tracking across the field of view.

In this study, we designed an asymmetric target model with equally spaced locally salient features. This is described by the *a priori* feature model geometry matrix $\mathbf{G} \in \mathbb{R}^{n \times 3}$, which consists of 3D coordinates in world space and will be used for kinematic model fitting in Section 2.2.2. Feature point coordinates $\mathbf{p}_i \in \mathbb{R}^2$ were automatically detected using multi-orientation kernel convolution with non-maxima suppression and sub-pixel localization [28]. Specifically, an interest point likelihood map was computed by convolving four feature kernels with the frame, and per-pixel feature likelihood was calculated by the maximum response over all prototype combinations. Sub-pixel feature localization was accomplished by solving a gradient orthogonality minimization problem:

$$\mathbf{p}_i = \arg \min_{\mathbf{q}_i} \sum_{\mathbf{n}_j \in \mathcal{N}(\mathbf{q}_i)} (\nabla_{\mathbf{q}_i}^T (\mathbf{n}_j - \mathbf{q}'_i))^2 \quad (4)$$

where \mathbf{q}_i is a feature coordinate candidate, $\mathcal{N}(\mathbf{q}_i)$ and $\nabla_{\mathbf{q}_i}$ are the pixel neighborhood and image gradient at point \mathbf{q}_i respectively, and \mathbf{n}_j is a neighboring pixel. Thus, $\mathbf{P} = \{\mathbf{p}_i\}$ describes the set of feature coordinates after undergoing optical projection onto the image plane according to the camera intrinsics \mathbf{K} . The (unknown) 3D orientation of the geometric model was estimated by fitting a kinematic model to these data, which is discussed next.

2.2.2 Kinematic Model Fitting

Given the set of 2D feature coordinate predictions \mathbf{P} , we fit a kinematic motion model of the *a priori* geometric model \mathbf{G} to these data. The kinematic model was designed to model the non-deformable nature of sway in free space with a fixed base of support. The model was parameterized by $\Theta = (\mathbf{t}, \mathbf{R})$, where $\mathbf{t} \in \mathbb{R}^3$ is 3D translation, and $\mathbf{R} \in \mathbb{R}^3$ are the Euler angles describing 3D orientation. The optimal kinematic

$$M_{\Theta} = \begin{bmatrix} \cos \Theta_1 \cos \Theta_2 & \cos \Theta_1 \sin \Theta_2 \sin \Theta_3 - \sin \Theta_1 \cos \Theta_3 & \cos \Theta_1 \sin \Theta_2 \cos \Theta_3 + \sin \Theta_1 \sin \Theta_3 & \Theta_4 \\ \sin \Theta_1 \cos \Theta_2 & \sin \Theta_1 \sin \Theta_2 \sin \Theta_3 + \cos \Theta_1 \cos \Theta_3 & \sin \Theta_1 \sin \Theta_2 \cos \Theta_3 - \cos \Theta_1 \sin \Theta_3 & \Theta_5 \\ -\sin \Theta_2 & \cos \Theta_2 \sin \Theta_3 & \cos \Theta_2 \cos \Theta_3 & \Theta_6 \\ 0 & 0 & 0 & 1 \end{bmatrix} \quad (7)$$

transformation, parameterized by these six degrees of freedom, was found by transforming the *a priori* geometric model into the image plane using the calibrated camera model, and seeking a least squares fit to the feature prediction data:

$$\hat{\Theta} = \arg \min_{\Theta} \sum_i \|\Pi(\mathbf{G}_i(\Theta)) - \mathbf{p}_i\|_2^2 \quad (5)$$

where Θ is the set of kinematic motion parameters, Π is the projection transformation from 3D world coordinates to the 2D image plane from Eq. (3), $\mathbf{G}_i(\Theta)$ are the transformed 3D coordinates of point i from the geometric model G , and \mathbf{p}_i is the feature prediction in image space.

This problem was solved using a two-step approach, consisting of an initializing and refinement step. To motivate this approach, we note that sway dynamics during quiet standing exhibit small and relatively smooth changes between each time point. In the first frame, we initialized the parameters Θ using a closed form planar estimation solution of the camera extrinsics [29]. In subsequent frames, noting that frame-to-frame sway differences are generally small (sub-millimeter), we set the initial conditions for the current frame (at time t_c) to the previous frame kinematic parameters ($\hat{\Theta}_{t_c-dt}$), and computed the optimal fit using Levenberg-Marquardt non-linear least-squares minimization. This approach avoided potential erroneous fits in local minima in other parts of the energy field, and we empirically found it produced higher accuracy than randomly initialized iterative optimization.

This optimization was performed on both the shoulder and lumbar targets separately, using their respective geometry priors. The target origin \mathbf{z}_u was used to track upper body motion. The torso kinematic parameters were used to project a virtual coordinate 10 cm deep into the body, which was used to track central motion:

$$\mathbf{z}_c = M_{\Theta} \Delta_l \quad (6)$$

where Δ_l is the torso vector in homogeneous world space coordinates, and M_{Θ} is the motion matrix parameterized by $\Theta \in \mathbb{R}^6$, described by Eq. (7).

2.2.3 Anatomical Space Transformation

To analyze posture sway patterns in anatomically relevant space, the kinematic parameters Θ were transformed from camera coordinate system into an anatomical coordinate system described by 1D axes (AP, ML, and SI) and derivative 2D planes (sagittal, transverse and coronal). A forward-facing calibration board was positioned in the scene, and its extrinsic orientation matrix was estimated using the calibration procedure from Section 2.2.1. Denoting this matrix as \mathcal{E} , sway in anatomical space coordinates was computed as:

$$\mathbf{z}'_u = \mathcal{E}^{-1} \mathbf{z}_u \quad (8)$$

$$\mathbf{z}'_c = \mathcal{E}^{-1} \mathbf{z}_c \quad (9)$$

where \mathbf{z}'_u and \mathbf{z}'_c are the shoulder and central sway coordinates in the anatomical coordinate system defined by \mathcal{E}^{-1} , the inverse of the planar target orientation in camera coordinates. The signals were denoised using a second order Savitzky-Golay filter [30] with 0.5 s time window, which empirically modeled the smooth nature of sway well.

2.3 Data Analysis

The interval between ECG R-waves was used to calculate heart rate (HR). Cardiac output (CO) was calculated as the product of HR and SV. Systolic blood pressure (SBP), diastolic blood pressure (DBP), and mean arterial pressure (MAP) were the respective maximum, minimum and mean arterial pressures within

each cardiac cycle. Identical analysis was performed to determine systolic, diastolic, and mean cerebral blood flow velocity (CBFv). $P_{ET}CO_2$ was determined by identifying the peak CO_2 concentration at the end of each exhalation, and the concentration was then converted to partial pressure. TSI was recorded at 50 Hz (Oxysoft, version 3.0.95, Artinis, Medical Systems, Elst, The Netherlands) and was averaged into 1 s bins. Beat-by-beat cardiovascular and breath-by-breath $P_{ET}CO_2$ data were linearly interpolated to 1 s time points, and subsequently time aligned with the cerebral oxygenation data for analysis. For all variables, supine baseline values were calculated as 30 s averages (from 45 s to 15 s before the posture transition). Early, mid, and late stance values were calculated as averages during the first 10 s of stance time.

To compare sway variations in control and hypoperfusion conditions, sway was divided and analyzed across three time bins spanning early, mid and late stance (0–20 s, 20–40 s, 40–60 s). For each time bin, the total path length in each anatomical axis (AP, ML, SI) and anatomical plane (transverse, sagittal, coronal) was computed as a summary metric for balance control [31]:

$$\mathcal{L}_{\mathcal{A}}(T) = \sum_{\tau_i \in T} \sqrt{(x_{i+1} - x_i)^2 + (y_{i+1} - y_i)^2} \quad (10)$$

where (x_i, y_i) are projected coordinates in the anatomical plane \mathcal{A} , and T is the stance time bin. \mathcal{L} within a 1D anatomical axis (i.e., AP, ML, SI) was computed by setting $y_i = 0$. This formulation is analogous to the average velocity magnitude during the time frame [32].

Two-way repeated measures ANOVA, with within-subject factors of condition (control vs hypoperfused) and time (baseline, early, mid, late stance), was performed on physiological measures. Normality was confirmed by the Shapiro-Wilks test, as well as visual inspection by using histograms and q-q plots of the residual distributions for each variable. Post hoc analysis was performed using paired sample t-tests to test differences across conditions within each time bin, and non-parametric ANOVA for non-normal sway TPL data [33, 34]. The p -values were adjusted via Bonferroni correction for assessing statistical significance. We reported statistically significant results when $p < 0.05$, and trending results when $p < 0.10$. Data are presented as mean \pm SEM.

3 Results

Section 3.1 presents accuracy validation of the monocular imaging system against a gold standard motion capture system. Section 3.2 presents repeated measures analysis of sway characteristics in control versus cerebral hypoperfusion across the relevant time bins. Video 1 shows the integration of cardiovascular response and postural sway estimation during a postural transition.

3.1 3D Estimation Accuracy

System accuracy was evaluated against a commercial active motion capture system with an accuracy of 0.1 mm and resolution of 0.01 mm (Optotrak, Northern Digital Inc, Canada). A subset of four participants (3/1 male/female) was used to validate system accuracy. Each participant stood quietly for 60 s across four trials to simulate different sway patterns: eyes open on foam, eyes closed on foam, eyes open on ground, eyes closed on ground. During “eyes open” stance, the participants looked at a visual target approximately 3 m in front at eye level. Three infrared emitting diodes were affixed to the same rigid bodies as the video camera targets. All motion tracking data were recorded simultaneously. Optotrak based kinematic data was sampled at 120 Hz, resampled to 30 Hz by linear interpolation to match the frame rate of the monocular kinematic system, and the coordinate system origins were aligned. For the purpose of this study, only the data from shoulder markers in the AP direction are discussed (similar results were observed for lumbar markers and ML displacements). Bland-Altman analysis was used to compare the two measurement systems. Specifically, all data were concatenated across participants for each of the kinematic systems, and the point-by-point differences were quantified through correlation and equality.

Figure 2 shows the agreement results between the proposed and motion capture systems. Bland-Altman analysis demonstrated no systematic error between the systems (error $4.4 \times 10^{-16} \pm 0.30$ mm), and no proportional error ($y = 1.01x + 8.4 \times 10^{-16}$, $r^2 = 0.9773$). The equality line fell within the confidence interval of the mean difference. Thus, the monocular imaging system demonstrated comparable postural sway tracking results to a whole-room gold standard method during quiet standing tasks.

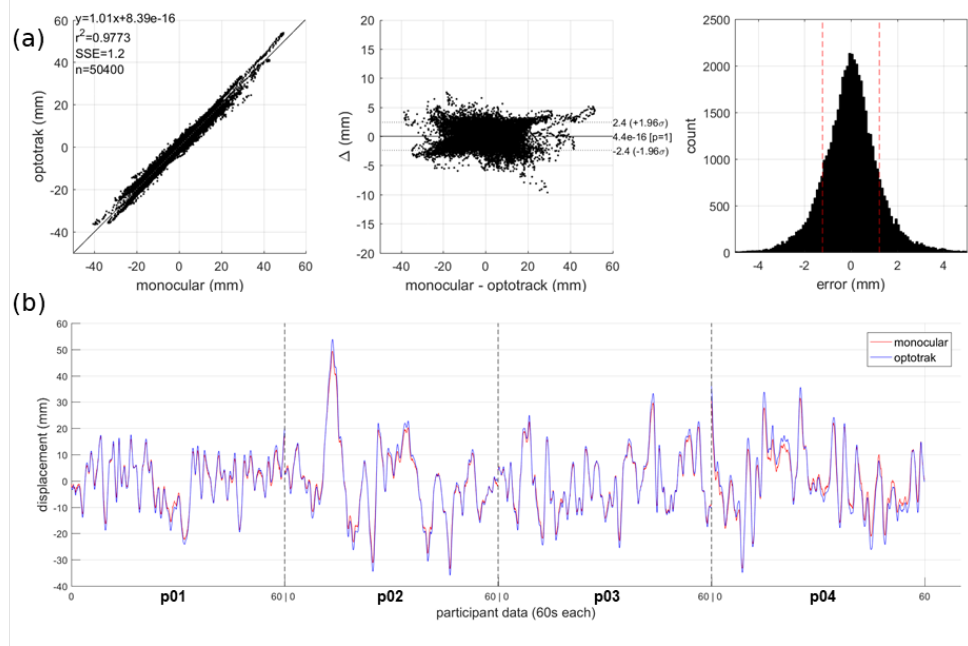


Figure 2: Accuracy of proposed monocular system compared to a whole-room motion capture system. (a) Bland-Altman analysis of systematic error shows strong agreement and sub-millimeter accuracy (error $4.4 \times 10^{-16} \pm 0.30$ mm). (b) Example monocular and Optotrak time series signals showing upper body anterior-posterior sway during 60 s quiet stand with eyes closed on foam.

3.2 Postural Sway and Cardiovascular Response

Both cardiovascular and sway showed the largest difference between control and hypoperfusion conditions during early stance, with gradual recovery to baseline by late stance, demonstrated by a significant main effect of time on all measures. Figure 3 shows the primary time-synchronized cardiorespiratory and cerebrovascular responses to standing (at $t = 0$) in both the control (blue) and hyperventilation (red) conditions. There were no significant main effects on perfusion condition in blood pressure measures (mean, diastolic, systolic), indicating preserved central arterial pressure across conditions. Significant Condition \times Time interaction terms were observed in all physiological measures, and are expanded and discussed below. Table 1 provides summary time-binned cardiovascular measures alongside statistical significances.

3.2.1 Hyperventilation Caused Hypoperfusion

Cerebral hypoperfusion was attained for each participant through hyperventilation-induced respiratory alkalosis. $P_{ET}CO_2$ was significantly lower in the hyperventilation compared to the control conditions during all time points ($p < 0.001$; see Table 1). In the hypoperfusion condition, $P_{ET}CO_2$ was a significant different across all stance times ($p < 0.001$) except from mid to late stance ($p = 0.43$). In the control condition, there were no significant differences in $P_{ET}CO_2$ across time points.

In both perfusion conditions, all participants demonstrated vasopressor response to upright posture with a transient reduction in blood pressure from baseline to early stance ($p < 0.001$), and compensatory increase in HR. There were no differences between conditions in systolic, diastolic, or mean blood pressure, hence between-condition differences in CBF and oxygenation were attributed to differences in $P_{ET}CO_2$ from hyperventilation. CBFv variables (systolic, diastolic, mean) and TSI all had significant Condition \times Time interaction effects due the compensatory mechanisms of CBFv after the termination of hyperventilation and acclimation to upright posture.

Figure 4 shows sway traces of a representative participant with CBF deficit during hyperventilation, and demonstrates the primary effects of standing on postural control. During early stance (blue), sway TPL increased in hypoperfused versus control (248.3 vs 166.2 mm). At this time, arterial blood pressure, CBFv

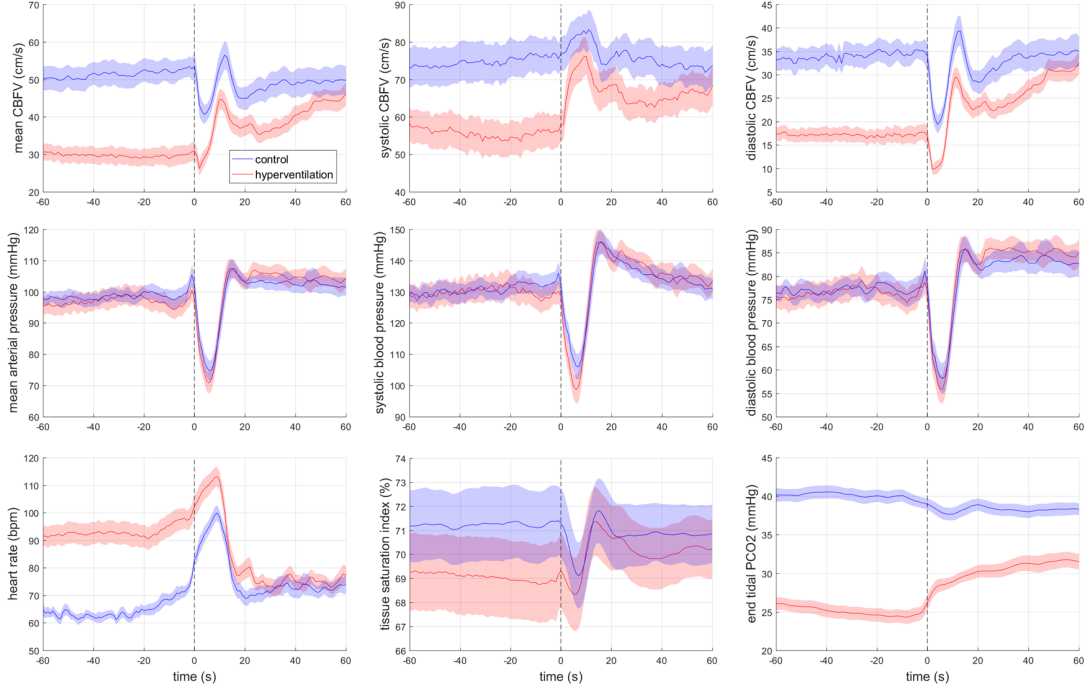


Figure 3: Cardiovascular response to standing during normal and reduced cerebral perfusion. Data were time-normalized based on established upright posture at $t=0$ s. Binned summary statistics are reported in Table 1. (CBFV: cerebral blood flow velocity; PCO_2 : partial pressure of carbon dioxide)

and TSI are transiently low due to active standing. During mid stance (green), the TPL difference between hypoperfused and control starts to diminish (151.9 vs 113.2 mm) as CBF and perfusion start to recover. By late stance (red), balance control had been re-established (132.5 vs 130.0 mm) owing to cerebral reperfusion and cardiovascular homeostasis. Whole-sample results binned by stance time are presented and discussed below. Figure 5 shows whole sample TPL distributions calculated across the relevant anatomical planes and anatomical axes for each time bin.

3.2.2 Early Stance

Significant between-condition reductions in all CBFv and oxygenation variables were observed in both baseline supine ($p < 0.001$) and early stance ($p < 0.03$), indicating acute onset of hypoperfused state during hyperventilation. Within the hypoperfusion condition, no significant differences were observed from baseline to early stance in mean CBFv or TSI, indicating sustained impaired cerebrovascular perfusion and oxygenation during the initial stance phase. A commensurate statistically significant increase in central anterior-posterior sway from control (147.1 ± 7.43 mm) to hypoperfusion (177.8 ± 15.3 mm) conditions was observed ($p = 0.039$), as well as trending differences in transverse (control: 183.3 ± 9.49 mm, hypoperfusion: 221.0 ± 19.4 mm; $p = 0.098$) and sagittal (control: 165.0 ± 8.34 mm, hypoperfusion: 200.3 ± 17.5 mm; $p = 0.075$) planes.

3.2.3 Mid Stance

During mid stance, significant reductions in all CBFv variables were observed ($p < 0.02$), but TSI was no longer statistically different ($p = 0.105$). Within the hypoperfusion condition, mean CBFv and TSI increased from early to mid stance ($p < 0.001$), indicating initial cerebral perfusion recovery onset. Anterior-posterior sway decreased, showing no significant trends in either central or upper body sway. However, significant differences were observed in upper body coronal sway (control: 106.3 ± 5.80 mm, hypoperfusion: 128.1 ± 18.4 mm; $p = 0.040$), and trending differences in both upper body (control: 90.3 ± 4.94 mm, hypoperfusion:

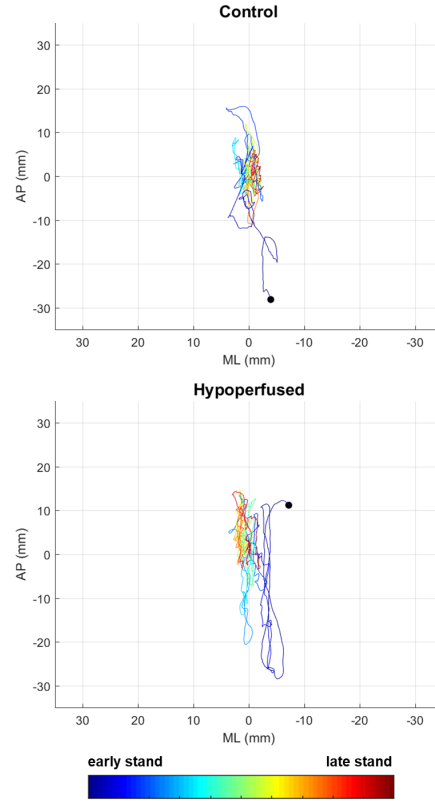


Figure 4: Example sway data of a participant with cerebral blood flow deficit during hypoperfusion. AP-ML only is shown for visual clarity. Standing in a hypoperfused state caused larger early (blue) and mid (green) stance sway dynamics compared to control. By late stance (red), sway stabilized in both conditions.

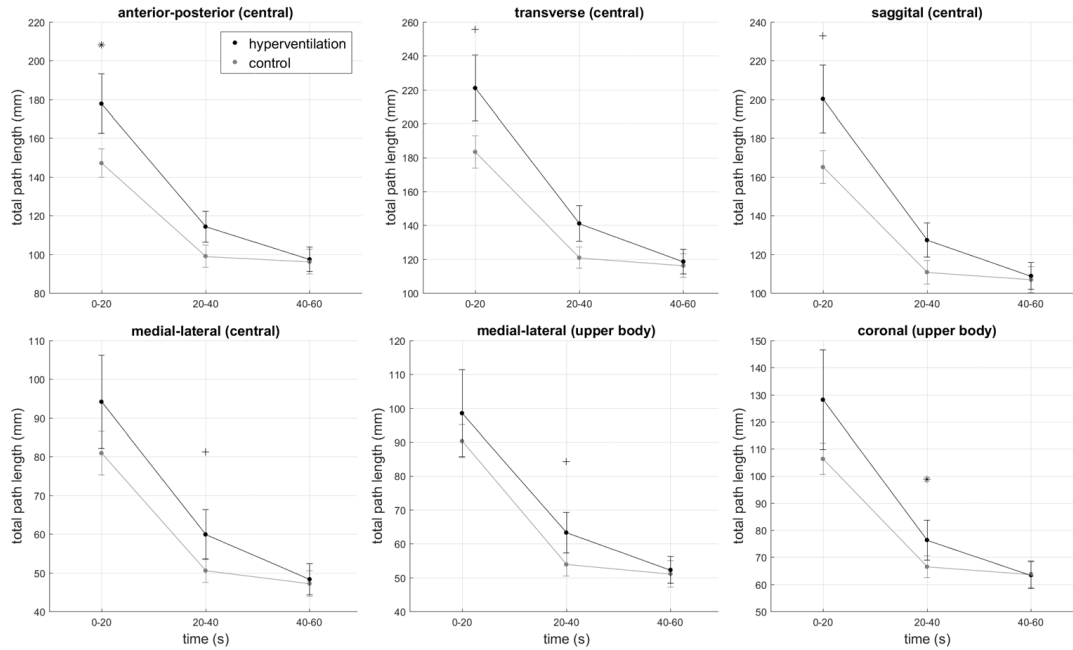


Figure 5: 3D sway binned across early, mid, and late stance times in the axes of anatomical motion and derivative motion planes. (* $p < 0.05$, + $p < 0.10$)

Table 1: Summary statistics of cardiovascular data binned by stance time (mean \pm SEM). Arterial blood pressure variables (MAP, SBP, DBP) did not show significant main effect differences on perfusion condition. All other variables showed significant main and interaction effects, indicating impaired cerebral blood flow and perfusion during hyperventilation. (HR: heart rate; MAP/SBP/DBP: mean/systolic/diastolic arterial blood pressure; SV: stroke volume; CO: cardiac output; CBFv: cerebral blood flow velocity; TSI: tissue saturation index; $P_{ET}CO_2$: end-tidal PCO_2)

| | Supine Baseline | | Early Stance | |
|---------------------|---------------------------------|----------------------------------|----------------------------------|-----------------------------------|
| | Control | Hypoperfusion | Control | Hypoperfusion |
| HR (bpm) | 63.1 \pm 1.6 ^b | 92.2 \pm 4.0 ^{*b,c,d} | 92.8 \pm 2.6 ^{a,c,d} | 108.5 \pm 3.8 ^{*a,c,d} |
| MAP (mmHg) | 98.6 \pm 2.1 ^b | 97.8 \pm 3.1 ^{b,c} | 83.1 \pm 3.1 ^{a,c,d} | 79.2 \pm 3.2 ^{a,c,d} |
| SBP (mmHg) | 130.6 \pm 3.0 ^b | 130.8 \pm 4.1 ^{b,c} | 114.6 \pm 3.6 ^{a,c,d} | 108.3 \pm 4.0 ^{a,c,d} |
| DBP (mmHg) | 77.3 \pm 1.9 ^{b,c,d} | 77.1 \pm 2.6 ^{b,c,d} | 64.4 \pm 3.1 ^{a,c,d} | 62.2 \pm 3.0 ^{a,c,d} |
| SV (mL) | 92.8 \pm 4.4 ^d | 90.9 \pm 3.8 ^{b,c,d} | 88.9 \pm 4.1 ^d | 79.9 \pm 4.3 ^{*a} |
| CO (L/min) | 5.8 \pm 0.3 ^b | 8.4 \pm 0.6 ^{*c,d} | 8.2 \pm 0.5 ^{a,c,d} | 8.6 \pm 0.6 ^{c,d} |
| Mean CBFv (cm/s) | 51.4 \pm 3.2 | 29.5 \pm 2.3 ^{*c,d} | 46.2 \pm 2.7 | 32.2 \pm 2.2 ^{*c,d} |
| Sys CBFv (cm/s) | 74.6 \pm 5.2 | 54.9 \pm 4.6 ^{*b,c,d} | 80.2 \pm 4.6 | 69.0 \pm 4.8 ^{*a} |
| Dia CBFv (cm/s) | 34.1 \pm 2.4 ^b | 17.1 \pm 1.5 ^{*b,c,d} | 25.9 \pm 2.0 ^{a,d} | 14.2 \pm 1.5 ^{*a,c,d} |
| TSI (%) | 73.2 \pm 1.0 ^b | 70.7 \pm 1.1 [*] | 71.3 \pm 1.3 ^a | 69.6 \pm 1.5 ^{*c} |
| $P_{ET}CO_2$ (mmHg) | 40.2 \pm 0.8 | 24.9 \pm 0.9 ^{*b,c,d} | 38.1 \pm 0.8 | 28.0 \pm 0.8 ^{*a,c,d} |

| | Mid Stance | | Late Stance | |
|---------------------|-------------------------------|----------------------------------|---------------------------------|----------------------------------|
| | Control | Hypoperfusion | Control | Hypoperfusion |
| HR (bpm) | 70.2 \pm 2.6 ^b | 76.3 \pm 2.8 ^{a,b} | 72.7 \pm 2.9 ^b | 75.1 \pm 2.6 ^{a,b} |
| MAP (mmHg) | 103.1 \pm 2.0 ^b | 105.6 \pm 2.5 ^{a,b} | 102.8 \pm 2.9 ^b | 104.2 \pm 2.9 ^b |
| SBP (mmHg) | 139.7 \pm 2.5 ^b | 141.0 \pm 3.3 ^{a,b,d} | 134.1 \pm 3.3 ^b | 134.6 \pm 3.8 ^{b,c} |
| DBP (mmHg) | 82.4 \pm 2.1 ^{a,b} | 84.9 \pm 2.1 ^{a,b} | 83.6 \pm 2.8 ^{a,b} | 85.1 \pm 2.4 ^{a,b} |
| SV (mL) | 88.4 \pm 5.7 ^d | 83.7 \pm 4.4 ^{a,d} | 78.1 \pm 4.8 ^{a,b,c} | 75.2 \pm 4.4 ^{a,c} |
| CO (L/min) | 6.2 \pm 0.4 ^{b,d} | 6.3 \pm 0.4 ^{a,b,d} | 5.7 \pm 0.4 ^{b,c} | 5.6 \pm 0.4 ^{a,b,c} |
| Mean CBFv (cm/s) | 46.5 \pm 3.1 | 36.7 \pm 2.4 ^{*a,b,d} | 49.3 \pm 3.6 | 42.1 \pm 2.5 ^{*a,b,c} |
| Sys CBFv (cm/s) | 76.4 \pm 4.4 | 65.7 \pm 4.5 ^{*a} | 73.7 \pm 5.0 | 65.2 \pm 4.6 ^{*a} |
| Dia CBFv (cm/s) | 30.2 \pm 2.5 ^d | 23.2 \pm 1.9 ^{*a,b,d} | 34.2 \pm 3.1 ^{b,c} | 28.7 \pm 2.0 ^{a,b,c} |
| TSI (%) | 72.0 \pm 1.2 ^d | 71.2 \pm 1.4 ^{b,d} | 71.7 \pm 1.2 ^c | 70.5 \pm 1.4 ^c |
| $P_{ET}CO_2$ (mmHg) | 38.5 \pm 0.8 | 30.3 \pm 0.8 ^{*a,b} | 38.1 \pm 0.8 | 31.3 \pm 1.1 ^{*a,b} |

* = significantly different from control condition value at a given time point (post-hoc analysis)

a,b,c,d = within-condition significantly different from supine baseline, early, mid, or late stance value, respectively.

98.6 \pm 12.9 mm; $p = 0.052$) and central (control: 80.9 \pm 5.69 mm, hypoperfusion: 94.2 \pm 12.1 mm; $p = 0.055$) medial-lateral sway.

3.2.4 Late Stance

During late stance, cerebral perfusion levels were largely recovered through no between-condition significant differences in diastolic CBFv or TSI, but mean CBFv and systolic CBFv remained low ($p < 0.04$). Within the hypoperfusion condition, cerebral perfusion continued to recover, demonstrated by significant increases in mean CBFv and TSI compared to mid stance ($p < 0.01$). There was no significant between-condition difference in any sway measures in late stance, indicating regained balance control following initial hypoperfusion onset.

4 Discussion

In this study we proposed a novel 3D monocular imaging system for monitoring postural sway in weakly constrained imaging environments. The system distinguished between upper body and central sway using two unique wearable targets with *a priori* geometric models. The sway was validated against a gold standard multi-camera whole room motion capture system during different postural tasks. Sway patterns linked to orthostatic hypotension were assessed using a hyperventilation protocol to acutely reduce cerebral perfusion prior to standing. Results showed significant differences in upper body and central sway patterns during early and mid stance between perfusion conditions, followed by similar sway patterns during late stance as

cerebral perfusion recovered.

We observed significant differences in sway commensurate with physiological changes in CBF and perfusion. Hyperventilation caused hypocapnia (reduced blood carbon dioxide) from forced exhalation, which results in vasoconstriction in cerebral vessels from the reduced partial pressure of CO_2 , and ultimately cerebral hypoxia [35]. Compensatory systemic effects were observed to compensate for the hypoxic condition. In healthy older adults, impaired cerebral vasoreactivity, but not impaired cerebral autoregulation, is associated with increased falls risk [36] primarily in the form of orthostatic intolerance (OI) [37]. Similarly, responses to head up tilt in OI groups following parabolic flight have been linked to cerebral vasoconstriction and not to systemic hypotension [38]. Similar responses have been observed in classic OI population, namely increased heart rate, decreased CBFv, and increased cerebrovascular resistance [39]. These manipulations demonstrate similar effects to traditional OI, and thus appear to be effective proxies for studying imbalance in older adults.

The increased heart rate observed while transferring from a supine to standing position was likely an effect of the acute gravitationally-driven drop in arterial blood pressure triggering the baroreflex [40]. The baroreflex response increases heart rate and total peripheral resistance in an attempt to maintain adequate arterial blood pressure. This effect was observed, where arterial pressures were well maintained across conditions. Baroreflex sensitivity decreases with age [41, 42], and has been linked to autonomic dysfunction, including orthostatic hypotension [43]. Current antihypertensive treatment for older adults living with orthostatic hypotension is governed by observations of decreased postural blood pressure [44]. Combining blood pressure data with functional measures of balance control may increase diagnostic aid and treatment efficacy.

Decreases in CBFv rather than blood pressure may provide better indications for postural instability and cerebral perfusion recovery. Whereas SBP dropped during the initial stages of standing, systolic CBFv was well maintained. Decreased systolic CBFv has been previously observed during pre-syncope [45]. The drops in mean and diastolic arterial blood pressure on standing were accompanied by reductions in CBFv that could impair O_2 delivery. Intact cerebrovascular autoregulation [36] promoted rapid recovery of CBFv associated with re-establishment of postural control by late stance following cerebral hypoperfusion.

Differences were observed for both central and upper body sway kinematics during the hypoperfused state support a multi-joint model of motion. Specifically, between condition differences during early stance were observed in central sway (anterior-posterior, transverse, sagittal), and mid stance were observed in both central (medial-lateral) and upper body (medial-lateral, coronal). Further studies are needed to expand these differences related to impaired neuromuscular control. There has been a wide range of body segmentation for assessing quiet standing, ranging from total body center of mass to individual rigid body segment (e.g., 14 segment bilateral model [25]). The current study evaluated a two-segment kinematic model, assuming hinging effects between upper and central body segments. Traditional body segment analysis requires placement of many optical markers on the body, and reconstruction of body segments using a multi-camera setup. The proposed system alleviates the setup load by distinguishing between upper and central body motion through two individual targets, which may reduce the barrier to adoption in clinical settings. Furthermore, since the imaging system tracks posterior anatomical markers, no facial information is recorded or required for 3D sway analysis, and thus participant or patient privacy can be maintained. This may be beneficial in home care and health care environments where privacy is an important factor in technology adoption [46].

5 Conclusion

In this paper, we proposed a novel monocular kinematic imaging system for assessing 3D postural sway during postural transition under varying cerebral perfusion levels. By physically embedding geometric priors, central and upper body kinematic motion was automatically tracked through feature tracking and 3D orientation inverse estimation. Central body sway was estimated by forward projecting a virtual coordinate midway through the body, and transforming the data into an anatomical coordinate system. The system was validated against a ground-truth motion capture system and demonstrated sub-millimeter accuracy across different types of sway. Hypocapnia-induced cerebral hypoperfusion showed increases in sway total path length in central anterior-posterior, transverse and sagittal motion during early stance, as well as increases in medial-lateral and coronal sway during mid stance. No differences were found during late stance, sug-

gesting recovered cerebral perfusion and neuromuscular control. This system provides inexpensive, accurate quantitative postural sway tracking in weakly constrained (non-laboratory) environments as a screening tool for cerebrovascular sufficiency and balance control in resource constrained settings.

6 Acknowledgments

This work was supported by the Natural Sciences and Engineering Research Council of Canada (PDF-503038-2017). The authors are grateful to Dr. Laura Fitzgibbon-Collins for her assistance with protocol development.

References

- [1] E. R. Kandel, J. H. Schwartz, T. M. Jessell, S. Siegelbaum, and A. Hudspeth, *Principles of Neural Science*, 5th ed. New York: McGraw-Hill, 2012.
- [2] D. A. Winter, “Human balance and posture control during standing and walking,” *Gait & Posture*, vol. 3, no. 4, pp. 193–214, 1995.
- [3] F. Bell, *Principles of Mechanics and Biomechanics*. Nelson Thornes, 1998.
- [4] S. W. Muir, K. Berg, B. Chesworth, N. Klar, and M. Speechley, “Quantifying the magnitude of risk for balance impairment on falls in community-dwelling older adults: a systematic review and meta-analysis,” *Journal of Clinical Epidemiology*, vol. 63, no. 4, pp. 389–406, 2010.
- [5] H. W. Lin and N. Bhattacharyya, “Balance disorders in the elderly: epidemiology and functional impact,” *The Laryngoscope*, vol. 122, no. 8, pp. 1858–1861, 2012.
- [6] L. Z. Rubenstein, “Falls in older people: epidemiology, risk factors and strategies for prevention,” *Age and Ageing*, vol. 35, no. suppl.2, pp. ii37–ii41, 2006.
- [7] M. Woollacott and A. Shumway-Cook, “Attention and the control of posture and gait: a review of an emerging area of research,” *Gait & Posture*, vol. 16, no. 1, pp. 1–14, 2002.
- [8] B. L. Edlow, M. N. Kim, T. Durduran, C. Zhou, M. E. Putt, A. G. Yodh, J. H. Greenberg, and J. A. Detre, “The effects of healthy aging on cerebral hemodynamic responses to posture change,” *Physiological Measurement*, vol. 31, no. 4, p. 477, 2010.
- [9] D. J. Mehagnoul-Schipper, L. C. Vloet, W. N. Colier, W. H. Hoefnagels, and R. W. Jansen, “Cerebral oxygenation declines in healthy elderly subjects in response to assuming the upright position,” *Stroke*, vol. 31, no. 7, pp. 1615–1620, 2000.
- [10] M. Gutkin and J. M. Stewart, “Orthostatic circulatory disorders: from nosology to nuts and bolts,” *American Journal of Hypertension*, vol. 29, no. 9, pp. 1009–1019, 2016.
- [11] L. Meng and A. W. Gelb, “Regulation of cerebral autoregulation by carbon dioxide,” *Anesthesiology: The Journal of the American Society of Anesthesiologists*, vol. 122, no. 1, pp. 196–205, 2015.
- [12] L. Sokoloff, “Relationships among local functional activity, energy metabolism, and blood flow in the central nervous system.” in *Federation Proceedings*, vol. 40, no. 8, 1981, pp. 2311–2316.
- [13] N. Goswami, A. P. Blaber, H. Hinghofer-Szalkay, and J.-P. Montani, “Orthostatic intolerance in older persons: etiology and countermeasures,” *Frontiers in Physiology*, vol. 8, p. 803, 2017.
- [14] C. Fortin, D. Ehrmann Feldman, F. Cheriet, and H. Labelle, “Clinical methods for quantifying body segment posture: a literature review,” *Disability and Rehabilitation*, vol. 33, no. 5, pp. 367–383, 2011.
- [15] A. Nardone and M. Schieppati, “The role of instrumental assessment of balance in clinical decision making,” *European Journal of Physical and Rehabilitation Medicine*, vol. 46, no. 2, pp. 221–237.

- [16] J. E. Visser, M. G. Carpenter, H. van der Kooij, and B. R. Bloem, "The clinical utility of posturography," *Clinical Neurophysiology*, vol. 119, no. 11, pp. 2424–2436, 2008.
- [17] A. Agustsson, M. Gislason, P. Ingvarsson, E. Rodby-Bousquet, and T. Sveinsson, "Validity and reliability of an iPad with a three-dimensional camera for posture imaging," *Gait & Posture*, vol. 68, pp. 357–362, 2019.
- [18] F. Wang, M. Skubic, C. Abbott, and J. M. Keller, "Body sway measurement for fall risk assessment using inexpensive webcams," in *2010 Annual International Conference of the IEEE Engineering in Medicine and Biology*, 2010, pp. 2225–2229.
- [19] D. Webster and O. Celik, "Systematic review of kinect applications in elderly care and stroke rehabilitation," *Journal of neuroengineering and rehabilitation*, vol. 11, no. 1, p. 108, 2014.
- [20] L. Yeung, K. C. Cheng, C. Fong, W. C. Lee, and K.-Y. Tong, "Evaluation of the Microsoft Kinect as a clinical assessment tool of body sway," *Gait & Posture*, vol. 40, no. 4, pp. 532–538, 2014.
- [21] F. Mueller, F. Bernard, O. Sotnychenko, D. Mehta, S. Sridhar, D. Casas, and C. Theobalt, "GANerated hands for real-time 3D hand tracking from monocular RGB," in *Proceedings of the IEEE Conference on Computer Vision and Pattern Recognition*, 2018, pp. 49–59.
- [22] L. Goncalves, E. Di Bernardo, E. Ursella, and P. Perona, "Monocular tracking of the human arm in 3D," in *Proceedings of IEEE International Conference on Computer Vision*, 1995, pp. 764–770.
- [23] P. Gagey, R. Gentaz, J. Guillamon, G. Bizzo, C. Bodot-Brgard, C. Debrulle, and C. Baudry, *Normes 85*, 2nd ed. Paris: Association Francaise de Posturologie, 1988.
- [24] A. E. Patla, M. G. Ishac, and D. A. Winter, "Anticipatory control of center of mass and joint stability during voluntary arm movement from a standing posture: interplay between active and passive control," *Experimental brain research*, vol. 143, no. 3, pp. 318–327, 2002.
- [25] W. H. Gage, D. A. Winter, J. S. Frank, and A. L. Adkin, "Kinematic and kinetic validity of the inverted pendulum model in quiet standing," *Gait & Posture*, vol. 19, no. 2, pp. 124–132, 2004.
- [26] Z. Zhang, "A flexible new technique for camera calibration," *IEEE Transactions on Pattern Analysis and Machine Intelligence*, vol. 22, 2000.
- [27] J. Heikkila and O. Silven, "A four-step camera calibration procedure with implicit image correction," in *Proc. Computer Vision and Pattern Recognition*, 1997, pp. 1106–1112.
- [28] A. Geiger, F. Moosmann, O. Car, and B. Schuster, "Automatic camera and range sensor calibration using a single shot," in *2012 IEEE International Conference on Robotics and Automation*, 2012, pp. 3936–3943.
- [29] Z. Zhang, "A flexible new technique for camera calibration," *IEEE Transactions on Pattern Analysis and Machine Intelligence*, vol. 22, 2000.
- [30] A. Savitzky and M. J. Golay, "Smoothing and differentiation of data by simplified least squares procedures," *Analytical Chemistry*, vol. 36, no. 8, pp. 1627–1639, 1964.
- [31] M. Salavati, M. R. Hadian, M. Mazaheri, H. Negahban, I. Ebrahimi, S. Talebian, A. H. Jafari, M. A. Sanjari, S. M. Sohani, and M. Parnianpour, "Test-retest reliability of center of pressure measures of postural stability during quiet standing in a group with musculoskeletal disorders consisting of low back pain, anterior cruciate ligament injury and functional ankle instability," *Gait & Posture*, vol. 29, no. 3, pp. 460–464, 2009.
- [32] R. A. Clark, A. L. Bryant, Y. Pua, P. McCrory, K. Bennell, and M. Hunt, "Validity and reliability of the Nintendo Wii balance board for assessment of standing balance," *Gait & Posture*, vol. 31, no. 3, pp. 307–310, 2010.

- [33] E. Brunner, S. Domhof, and F. Langer, *Nonparametric analysis of longitudinal data in factorial experiments*. Wiley-Interscience, 2002, vol. 406.
- [34] K. Noguchi, Y. R. Gel, E. Brunner, and F. Konietzschke, “nparLD: an R software package for the nonparametric analysis of longitudinal data in factorial experiments,” *Journal of Statistical Software*, vol. 50, no. 12, 2012.
- [35] V. Sakellari, A. Bronstein, S. Corna, C. Hammon, S. Jones, and C. Wolsley, “The effects of hyperventilation on postural control mechanisms,” *Brain*, vol. 120, no. 9, pp. 1659–1673, 1997.
- [36] F. Sorond, A. Galica, J. Serrador, D. Kiely, I. Iloputaife, L. Cupples, and L. A. Lipsitz, “Cerebrovascular hemodynamics, gait, and falls in an elderly population: Mobilize boston study,” *Neurology*, vol. 74, no. 20, pp. 1627–1633, 2010.
- [37] V. Gupta and L. A. Lipsitz, “Orthostatic hypotension in the elderly: diagnosis and treatment,” *The American journal of medicine*, vol. 120, no. 10, pp. 841–847, 2007.
- [38] J. Serrador, J. Shoemaker, T. Brown, M. Kassam, R. Bondar, and T. Schlegel, “Cerebral vasoconstriction precedes orthostatic intolerance after parabolic flight,” *Brain Research Bulletin*, vol. 53, no. 1, pp. 113–120, 2000.
- [39] V. Novak, J. M. Spies, P. Novak, B. R. McPhee, T. A. Rummans, and P. A. Low, “Hypocapnia and cerebral hypoperfusion in orthostatic intolerance,” *Stroke*, vol. 29, no. 9, pp. 1876–1881, 1998.
- [40] L. B. Rowell, *Human Cardiovascular Control*. Oxford University Press, 1993.
- [41] B. Gribbin, T. G. Pickering, P. Sleight, and R. Peto, “Effect of age and high blood pressure on baroreflex sensitivity in man,” *Circulation Research*, vol. 29, no. 4, pp. 424–431, 1971.
- [42] L. Korner, A. P. Hoeks, B. J. Janssen, A. J. Houben, P. W. De Leeuw, and R. S. Reneman, “Neural activity of the cardiac baroreflex decreases with age in normotensive and hypertensive subjects,” *Journal of Hypertension*, vol. 23, no. 4, pp. 815–823, 2005.
- [43] P. A. Low and V. A. Tomalia, “Orthostatic hypotension: mechanisms, causes, management,” *Journal of Clinical Neurology*, vol. 11, no. 3, pp. 220–226, 2015.
- [44] M. A. James and J. F. Potter, “Orthostatic blood pressure changes and arterial baroreflex sensitivity in elderly subjects,” *Age and Ageing*, vol. 28, no. 6, pp. 522–530, 1999.
- [45] K. N. Thomas, J. D. Cotter, S. D. Galvin, M. J. Williams, C. K. Willie, and P. N. Ainslie, “Initial orthostatic hypotension is unrelated to orthostatic tolerance in healthy young subjects,” *Journal of Applied Physiology*, vol. 107, no. 2, pp. 506–517, 2009.
- [46] K. Arning and M. Ziefle, ““Get that camera out of my house!” Conjoint measurement of preferences for video-based healthcare monitoring systems in private and public places,” in *International Conference on Smart Homes and Health Telematics*, 2015, pp. 152–164.